ELSEVIER

Deformities in larval gilthead sea bream (*Sparus aurata*): A qualitative and quantitative analysis using geometric morphometrics

Yves Verhaegen [a], Dominique Adriaens [a,*], Tania De Wolf [b],
Philippe Dhert [c], Patrick Sorgeloos [d]

[a] *Evolutionary Morphology of Vertebrates, Ghent University, K.L. Ledeganckstraat 35, B-9000 Gent, Belgium*
[b] *Maricoltura di Rosignano Solvay, srl, Via P. Gigli (Loc Lillatro), I-57013 Rosignano Solvay, Italy*
[c] *INVE Technologies, NV, Oeverstraat 7, B-9200 Baasrode, Belgium*
[d] *Laboratory of Aquaculture and Artemia Reference Center, Ghent University, Rozier 44, B-9000 Gent, Belgium*

Abstract

Deformities in commercially raised fish are a common source of downgrading of product value. During the intensive rearing of gilthead sea bream (*Sparus aurata*), opercular deformities are the most commonly observed type of deformation (affecting up to 80% of the fisheries stock), sometimes showing a severe inward folding of the operculum. They are non-lethal malformations that appear during the larval stage but affect growth rate and morphology, with a significant economic loss as a consequence. In order to exploratory quantify and qualify these deformities, geometric morphometric analyses were performed on the external morphology from larvae with an age ranging from 50 to 69 days post-hatching (DPH), and on the cranial skeleton of 110 DPH old juveniles. The results showed several osteological cranial shifts and a striking left–right independency associated with deoperculation. Even though a significant size difference was observed at 65 DPH between normal and deoperculated specimens, allometrics during the examined growth stages still appear to be very similar in normal and deoperculated specimens. At 69 DPH deoperculated specimens differed significantly from the normal specimens in their external morphology based on its shape variables, but the results suggest that discrimination is possible from earlier stages. Further analyses are needed, but the usefulness of this approach towards developing an early detection tool could be demonstrated.
© 2007 Elsevier B.V. All rights reserved.

Keywords: Sparus aurata; Opercular complex; Abnormality; Geometric morphometrics; Ontogeny

1. Introduction

Gilthead sea bream (*Sparus aurata*), being one of the first intensively cultivated species in the Mediterranean (Fishery Information, Data and Statistics Unit, Food and Agriculture Organization of the United Nations (FAO), 2005), has become an important research topic over the years (Koumoundouros et al., 1997a). The focus has mainly been on aquacultural aspects, and the implementation of techniques to improve reproductive success, survival and growth (Tandler and Helps, 1985; Polo et al., 1991; Mourente et al., 1993; Parra and Yufera, 2000; Papandroulakis et al., 2002; Sadek et al., 2004). As a maximal yield in growth and reproductive success may come into reach, problems arise with respect to the overall quality (especially deformations) of the fry and subsequent juvenile fish. Although some studies on larval quality have been performed in the past (*e.g.* Papema,

* Corresponding author. Tel.: +32 9 264 52 19; fax: +32 9 264 53 44.
E-mail address: dominique.adriaens@ugent.be (D. Adriaens).

1978; Koumoundouros et al., 1995; Furuita et al., 2000; Boglione et al., 2001; Cahu et al., 2003), future research efforts may need to concentrate even more on a qualitative rather than quantitative improvement of the produced fish, especially in order to expose the nature behind developmental and growth problems frequently experienced in cultivating facilities. Some examples of common abnormalities in cultivated fish are axial deformities, whether or not related to swimbladder abnormalities (such as saddle-back syndrome and axial lordosis) (*e.g.* Alfonso et al., 2000, Boglione et al., 2001), abnormal caudal fin development (*e.g.* Koumoundouros et al., 1997b) and opercular deformations. Especially the distorted development of the operculum in *S. aurata*, as well as in some other cultivated species, have been a source of product downgrading and substantial economic losses over many years (affecting up to 80% of farmed gilthead sea bream) (Paperna, 1978; Francescon et al., 1988; Chatain, 1994; Andrades et al., 1996).

In order to improve cost-efficiency for farmed market-sized gilthead sea bream, a fast and early recognition of developing abnormalities is of utmost importance for fish farmers, as well as to unravel the effect of rearing parameters in order to minimize the prevalence of these deformities a priori. As a result, research efforts have been focusing on biometric screening of larvae for such deformities (Koumoundouros et al., 1997a). However, studying the pattern behind deformities and related growth disturbances is frequently based on biometric analysis, relying on point-to-point measurements of several structures and parts of the body plan (Koumoundouros et al., 1997a; Lindesjöo et al., 1994). Such an approach is useful for studying size changes, thus growth, but is insufficient in describing aspects of shape adequately (especially size-independent shape, even when using ratios) (see Richtsmeier et al., 2002; Dodson, 1978), thus possibly problematic when studying deformities. For that reason, geometric morphometrics allow a more complete description of shape and thus a more robust and detailed analysis of shape variation in growing and transforming fishes (Rohlf and Marcus, 1993; Adams et al., 2004). This approach has proven to be useful for studying shape changes of commercially important fishes in the past (*e.g.* Cavalcanti et al., 1999; Koumoundouros et al., 2005; Loy et al., 1998; 2000; 2001; Valentin et al., 2002), including *S. aurata* (Loy et al., 1999). All these shape analyses focused on populations in the wild, or the effect of rearing conditions on the overall body shape in adult specimens.

We performed a landmark-based geometric morphometric analysis on both external and internal (skeletal) morphology of different age groups of *S. aurata*. The specific goals of this exploratory study are: (1) to analyze quantitatively and qualitatively the nature of osteological aberrations in the skull associated with deoperculation in 110 day old juveniles, and (2) to verify to what degree shape changes in the external morphology (total body shape) co-occur with opercular deformities between 50 and 69 days post-hatching. Such an approach will assist in future efforts to allow a fast recognition protocol for detecting early opercular deformation in cultivated gilthead sea bream.

2. Material and methods

2.1. Rearing conditions

All specimens originate from the commercial sea bream hatchery Maricoltura di Rosignano Solvay (Italy). Eggs were obtained from a mixed broodstock of reared and locally wild caught adults. The broodstock was fed a mixed diet of Lansy Breed[th] (INVE Aquaculture NV, Belgium) pellets and fresh seafood (shrimps, mussels, crabs and fish). Spawning occurred under regulated light and temperature conditions in 2800 l tanks. The collected eggs hatched in a 140 l incubation tank approximately 48 h after spawning and were transferred indoors to 6000 l larval rearing tanks after 24 h. Initial rearing density was approximately 150 larvae/l. Larvae were raised under a semi-closed circuit of filtered natural seawater (39% salinity) originating from the nearby coast. Temperatures and dissolved oxygen concentrations were continuously kept closely to 19 °C and between 6–12 ppm, respectively. The following light intensity regime were applied: 0–1 DPH at 80 lx. 2–3 DPH at 250, 4–13 DPH at 400, 14–39 DPH at 250 lx and subsequent weaning at natural shaded sunlight (4000 lx). High aeration during 0–1 DPH kept passively moving larvae suspended, with aeration at low level during green water phase (sufficient to distribute algae over water column). After this phase passive aeration induced by water flow was sufficient. The creation of water currents was minimized through the vertical position of the water inlet just above the water surface to allow a natural swimming behaviour of the developing fish. As from 48 DPH, the post-metamorphic phenomenon of schooling was prevented by placing a vertically submerged net in the circular tanks.

Surface skimmers were used to inhibit lipid film formation on the water surface (Chatain and Ounais-Guschemann, 1990). The 'green water' technique was applied during the period 3–28 DPH, using two phytoplankton strains (*Nannochloropsis sp.* and *Isochrysis sp.*). The larvae were fed live feed starting on day three

(successively with *Brachionus sp.* Biotype Cayman, INVE *Artemia* AF strain and INVE *Artemia* EG strain) followed by INVE Proton 1, Proton 2/3 and Proton 2/4 artificial diets. After 48 DPH the batch was separated in two fractions, using a grader with 1.5 mm mesh-size, and then transferred separately to 10,000 l weaning tanks.

2.2. Samples

For the osteological analysis, eleven normal and ten deoperculated specimens were sampled from a batch of 110 DPH old juveniles on the 11th of March 2004. We will apply the term "deoperculation" for any kind of deformation where the operculum shows microscopically visible signs of opercular reduction or shape distortions. For the external morphology, a total of 433 specimens were sampled at seven time intervals (41, 45, 50, 55, 61, 65 and 69 DPH) during the period December 6th 2004 till January 3rd 2005, each sample consisting of 31–120 specimens and representing a total standard length (L_S) range of 7.2–22.0 mm. Furthermore, five wild caught larvae (17.3–18.0 mm L_S) were obtained from a local fisherman.

All sampled specimens were anaesthetized using an overdose of MS-222 (>100 ppm) and were fixed and stocked separately in a 4% NaH_2PO_4–Na_2HPO_4 buffered formalin.

A whole-mount clearing and staining of the 21 juveniles, sampled for the osteological analysis of the skull and pectoral girdle, was carried out using the methods of Hanken and Wassersug (1981) and Taylor and Van Dyke (1985). Both lateral views of all specimens were photographed using a Colorview 8 digital camera mounted on an Olympus SXZ-9 stereoscopic microscope, with analysis Docu 3.00 (Soft Imaging System GmbH) software. Before being photographed, specimens were positioned as perfectly lateral as possible using the overlap of paired anatomical structures as an important guidance, in order to minimize possible shape variation due to suboptimal positioning. 50 of the 433 specimens for the external morphology analysis couldn't be positioned adequately because of an abnormal flexion of the body (natural and/or through fixation), and were thus omitted from further analysis. As no reliable markers for the body midline could be discerned on the early larval stages, the unbending module in tpsUtil was not performed (Rohlf, 2004a). All photographs of the right body sides where then mirrored in order to allow the comparison of left and right sides in a single analysis. Standard lengths (L_S) were measured on the digital images using analysis Docu 3.00 (Soft Imaging System GmbH) software. The nomenclature used to describe the skeletal structures is based on Faustino and Power (2000).

2.3. Landmark data

Landmark data were gathered using tpsUtil (Rohlf, 2004a) to construct the tps-files and tpsDig for digitising landmark positions on the digital images (Rohlf, 2004b) (freeware at http://life.sunysb.edu/morph). For the two datasets, a set of homologous landmarks was digitised in two dimensions. Landmarks chosen were so-called type 1 and type 2 landmarks, thus allowing a reliable representation of the actual shape variation (instead of measuring error noise) (for a definition of these two types, see Bookstein, 1990). An estimation of digitising and orientation error, however, was performed (see below). The osteology dataset included a total of 21 homologous landmarks that were digitised bilaterally on the 21 specimens, thus yielding 42 landmark configurations to be analysed (Fig. 1). Landmarks were chosen in order to have a good representation of the overall skull shape with respect to the vertebral column, but especially with a detailed representation of the opercular region. Following landmarks were used: (1) the anteroventral tip of the premaxillary bone (type 2), (2) the caudal tip of the premaxillary bone (type 2), (3) the anterior tip of the dentary bone (type 2), (4) the mediodorsal suture between nasal and frontal bone (type 1), (5) the dorsal point of contact between infraorbital bones three and four (type 1), (6) the anterodorsal tip of the sphenotic (type 1), (7) the posterodorsal tip of the supraoccipital bone (type 2), (8) the posterior tip of the post-temporal bone (type 2), (9) the posterodorsal tip of the preopercular bone (type 2), (10) the posterodorsal tip of the opercular bone (type 2), (11) the caudal tip of the opercular bone (type 2), (12) the ventral tip of the opercular bone (type 2), (13) the posterior tip of the subopercular bone (type 2), (14) the ventral end of the contact zone between subopercular and interopercular bone (type 1), (15) the anterior tip of the interopercular bone (type 2), (16) the overlap of the subopercular–interopercular bone suture with the posterior margin of the preopercular bone (type 1), (17) the anterior tip of the preopercular bone (type 2), (18) the ventral tip of the cleithrum (type 2), (19) the caudal tip of the cleithrum (type 2), (20) the anterior tip of the neural arch of the third vertebra (type 2), (21) the anterior tip of the neural arch of the fifth vertebra (type 2).

The external morphology dataset shape model relied on a total of 16 landmarks (Fig. 2). Specimens smaller than 11.4 mm L_S (all specimens younger than 50 DPH and three specimens aged 50 DPH) were further omitted from the geometric morphometric analysis because of a lack of landmarks that could be homologised on these specimens. Of the 310 specimens left and right sides were digitised and analysed

separately (as most landmarks in both views were identical as they were positioned in the medial plane), yielding two datasets (left and right). Again, landmarks were of type 1 and 2, with the exception of one (landmark 15). Landmarks were chosen to represent the overall body shape, as well as the position of the pectoral fin, the back of the skull and the eye. As specimens were categorised as normal or deoperculated based on visible abnormalities in the opercular region, the shape model of the external morphology did not include landmarks in the opercular region, thus allowing an independent analysis of shape changes co-occurring with deoperculation. Following landmarks were used: (1) the anterodorsal tip of the premaxillary (type 1), (2) the posterior border of the skull (type 1), (3) the base of the first spine of the dorsal fin (type 2), (4) the base of the first soft ray of the dorsal fin (type 2), (5) the base of the last soft ray of the dorsal fin (type 2), (6) the dorsal onset of the caudal fin (type 1), (7) the midlateral posterior edge of the peduncle (type 2), (8) the ventral onset of the caudal fin (type 1), (9) the base of the last ray of the anal fin (type 2), (10) the base of the first ray of the anal fin (type 2), (11) the base of the pelvic fin (type 1), (12) the posteroventral tip of the mandibular (type 1), (13) the base of the last (upper) ray of the pectoral fin (type 2), (14) the base of the first (lower)

ray of the pectoral fin (type 2), (15) the centre of the eye (type 3), (16) the posterior tip of the skull (type 1).

2.4. Morphometrics

In order to remove all variation in size, rotation and position (with respect to the image frame), a standardisation was done for all three parameters. For that, a Generalised Procrustes Analysis (GPA) was performed where all landmark configurations were scaled to the same centroid size ($CS=1$), aligned with centroids being superimposed and rotated until a maximal fit of homologous landmarks (Rohlf and Slice, 1990). This yields a dataset reflecting only differences in true shape. Shape differences were calculated between all specimens, as well as between all specimens and a consensus (i.e. an average landmark configuration of all specimens in the dataset). The fitness of the dataset for further statistical analysis was tested using tpsSmall (Rohlf, 2003), so that the distribution of shape distances in the non-Euclidean Kendall shape space (i.e. Procrustes distances) between specimens is properly represented in the Euclidean tangent space (i.e. tangent distances) (for a discussion on these shape spaces, see Rohlf, 1996). All datasets proved to be fit for analysis (correlation between Procrustes distances and tangent distances was 1.0000).
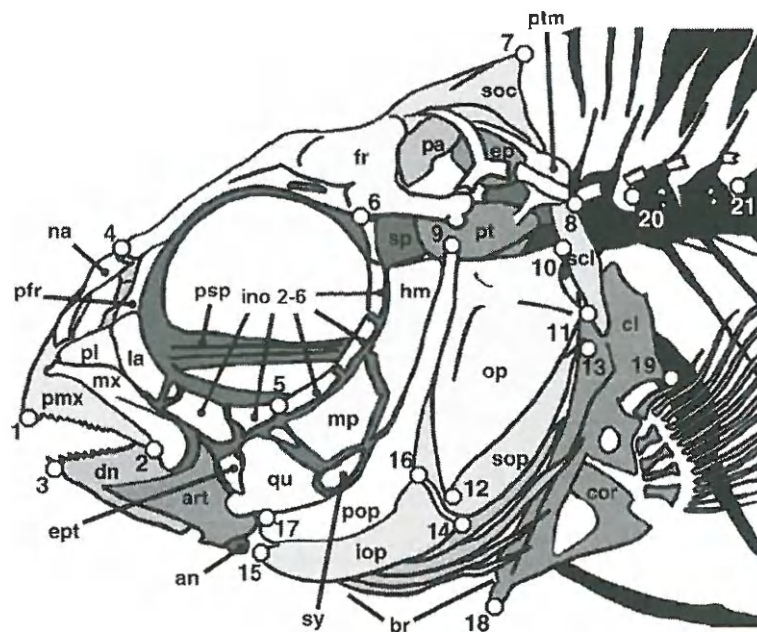

Fig. 1. Drawing of the cranial osteology and the landmarks applied. an, angular; art, articular; br, branchiostegal rays; cl, cleithrum; cor, coracoid; dn, dentary; ept, ectopterygoid; ep, epiotic; fr, frontal; hm, hyomandibular; ino 2–6, infraorbital two to six; iop, interopercular; la, lacrimal; mp, metapterygoid; mx, maxilla; na, nasal; op, opercular; pa, parietal; pfr, prefrontal; pl, palatine; pmx, premaxilla; pop, preopercular; psp, parasphenoid; pt, pterotic; ptm, posttemporal; qu, quadrate; scl, supracleithrum; soc, supraoccipital; sop, subopercular; sp, sphenotic; sy, symplectic.
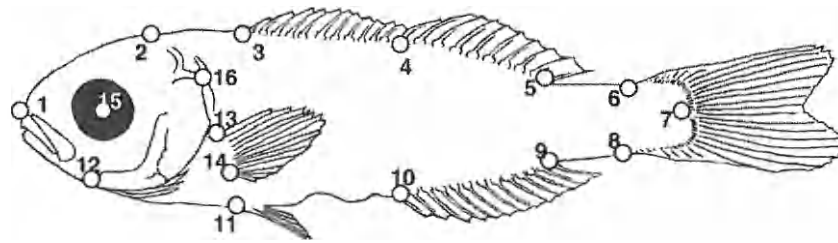
Fig. 2. Drawing of the external morphology of a large 50 DPH old specimen (13.9 mm L_S) and the landmarks applied.

2.5. Error analysis

Since both larval and juvenile specimens were laterally flattened, measuring error as a result of a reduction in dimensions was minimal (for a discussion on measuring errors in geometric morphometrics, see Arnqvist and Mårtensson, 1998). A separate error analysis was done to estimate the amount of error induced by the action of digitising, as well as that as a result of variation in positioning the specimens for imaging. An estimate of digitising error was done by digitising ten times the same image from a single specimen of the osteological data (all specimens had a comparable size) and from two specimens (the largest and smallest) from the external morphology data. The estimate of artificial shape variation as a result of variation in the positioning of the specimens was done by
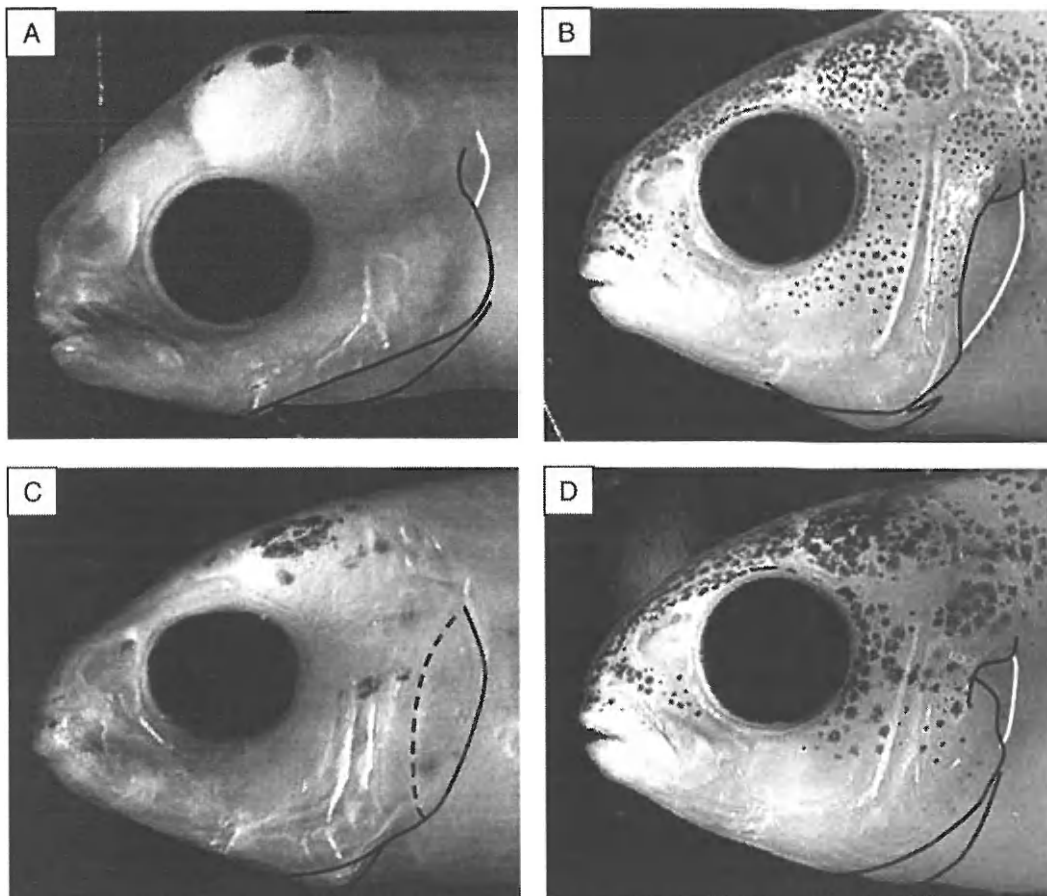

Fig. 3. External morphology of the head region, showing the onset of deoperculation. A. Early opercular deformation in a 40 DPH, 8.5 mm L_S post-larva; B. severe stage of opercular deformation in a 69 DPH, 19.5 mm L_S juvenile; C. aberrant type of opercular deformity in a 55 DPH, 14.7 mm L_S juvenile; D. aberrant type of opercular deformity in a 69 DPH 18.4 mm L_S juvenile. Black lines indicate the caudal edge of the operculum and branchiostegal rays, white lines mark the caudal edge of the gill cavity. The crest of an abnormally light folding is indicated by a dashed black line in Fig. 3C.
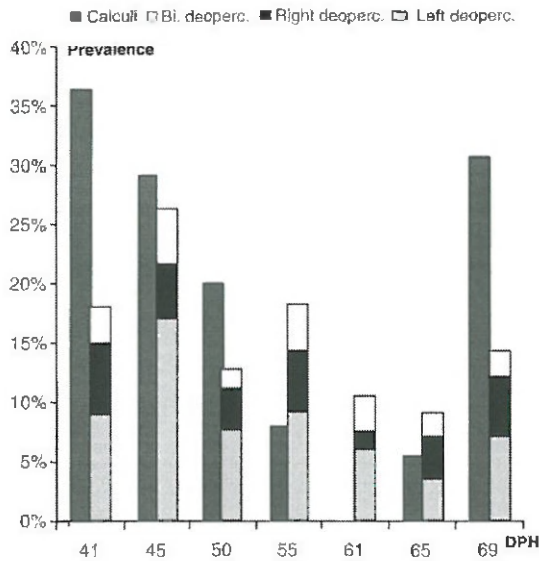
Fig. 4. Prevalence of urinary calculi and opercular deformities, for all studied age classes.

using these three specimens, but which were now positioned and photographed ten times repeatedly.

The average Procrustes distances of these datasets were then expressed as percentage of these distances of the total dataset, revealing an estimate of the amount of shape variation which can be attributed to digitising and positioning errors.

2.6. Statistical analyses

Variables describing shape variation (*i.e.* partial warps) in the datasets, based on the 2D-coordinates, were calculated using tpsRelw (Rohlf, 2005). For the

statistical analysis, both uniform and non-uniform partial warps were included. The obtained matrices of partial warp scores of all specimens (weight matrix) in both datasets were subsequently submitted to a Principal Component Analysis (also called a Relative Warp analysis when using partial warp scores) (Rohlf, 1993). By doing so, the total shape variation was decomposed into a new set of variables (*i.e.* relative warps) that describe the most important variation in the datasets. This was also done using tpsRelw, which was also used to generate deformation grids to visualise the explained shape variation (with respect to the consensus configuration). Scaling was set equal ($\alpha = 0$) for local and diffuse non-uniform shape changes (Rohlf, 1993; Rohlf et al., 1996).

For the external morphology dataset, a discriminant function analysis (DFA) was performed on the shape variables (using the weight matrix) to test the significance of existing differences between normal and deoperculated specimens for the different length and age classes (Statistica 6, Statsoft Inc.). As mentioned, a priori discrimination between normal and deoperculated specimens was performed by a microscopical analysis of the opercula. Both canonical scores, as well as relevant statistical parameters (Squared Mahalanobis distance, *F*-value and *p*-levels) were calculated using Statistica 6.0 (Statsoft, Inc.). For all statistical analyses, *p*-levels smaller than 0.05 were considered as significant. The shape changes associated with the canonical variates were visualised using tpsRegr (Rohlf, 2004c), including a randomisation test (with 1000 permutations).

As centroid size correlated highly with the measured standard lengths ($R^2 > 0.98$,) we preferred the latter as size parameter, because it can be more easily obtained during the daily monitoring of stocks in fish farms.

Fig. 5. Consensus configuration of the osteological dataset, with differences in landmark position of aligned specimens indicated as vectors.

Table 1
Percent of variation explained by the first ten relative warps of the osteological and both external morphology datasets

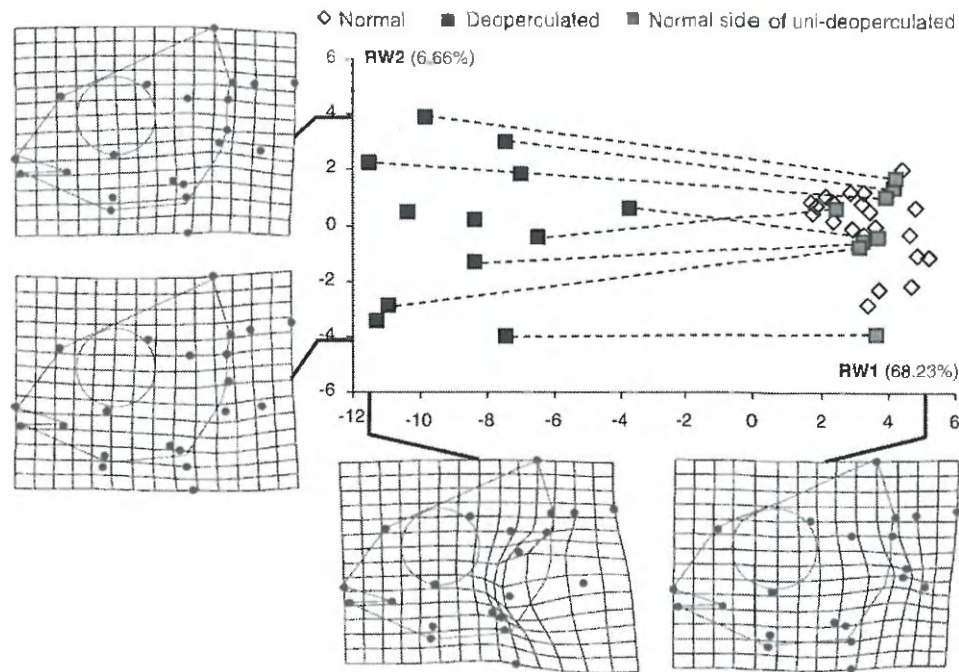| RW	% of variation explained		
	Osteology	Left external	Right external
1	68.23%	51.52%	54.00%
2	6.66%	10.42%	9.42%
3	5.56%	7.79%	7.02%
4	3.46%	4.45%	4.42%
5	2.63%	3.67%	3.25%
6	2.06%	3.29%	2.98%
7	1.70%	2.74%	2.53%
8	1.54%	2.23%	2.22%
9	1.39%	1.76%	1.90%
10	0.95%	1.69%	1.55%

Fig. 6. Scatter plot of relative warp 1 versus relative warp 2 scores, showing a separate clustering of the normal (diamonds) and abnormal specimens (filled squares). The normal sides of the skull of unideoperculated fishes clearly fall into the normal cluster (empty squares). Dotted lines interconnect normal and abnormal sides of unilaterally deoperculated specimens. Shape variation explained by the relative warps is visualised by the deformation grids (showing the shape differences with respect to the consensus).

2.7. Calculation of inflection points

In order to objectively calculate the most significant shifts in shape changes (expressed as relative warp 1) versus size (log L_S), inflection points were calculated as proposed by Van Snik et al. (1997): the data was log-transformed, regression lines were calculated for x_{min} until $x_{intermediate}$, and for $x_{intermediate}$ to x_{max}, where $x_{intermediate}$ was a variable iteratively ranging from x_{min+2} to x_{max-2}. T-tests were done to check whether the group
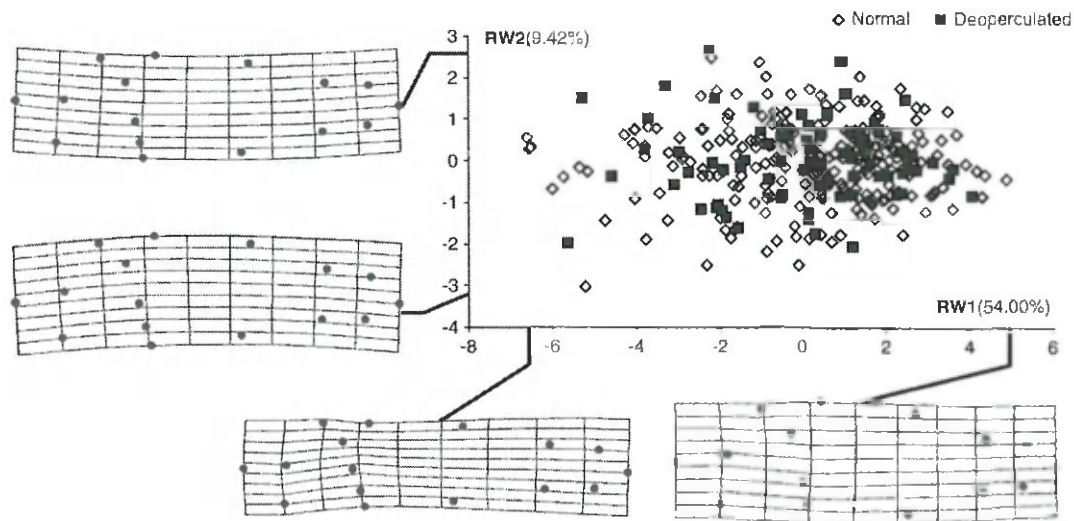

Fig. 7. Scatter plot of relative warp 1 versus relative warp 2 scores of the analysis of the right body side, showing the overlap of the normal (diamonds) and abnormal specimens (squares). Shape variation explained by the relative warps is visualised by the deformation grids (showing shape difference with respect to consensus, mirrored).
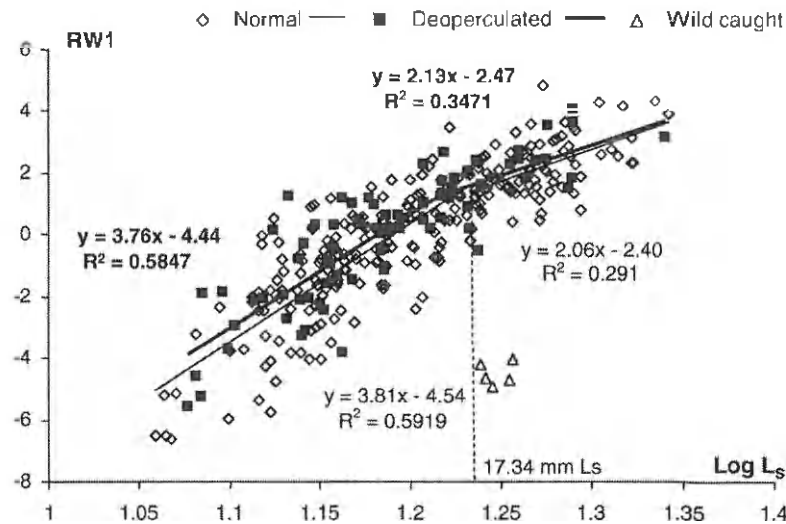
Fig. 8. Scatterplot of RW1 versus body size (log-transformed L_S) of the analysis of the right body side, with the indication of the calculated inflection point.

of growth coefficients for x_{min} to $x_{intermediate}$ significantly differs from the group of growth coefficients for $x_{intermediate}$ to x_{max}. The $x_{intermediate}$ value that shows the largest significant t-stat is defined as the inflection point.

3. Results

3.1. Size and deoperculation

Opercular deformities were already visually detectable in the smallest and youngest specimens (8.0 mm L_S, 40 DPH) as a small notch dorsally in the free opercular edge (Fig. 3A shows an 8.5 mm L_S, 40 DPH specimen). During this phase the operculum is still largely unossified and a large posteroventral part is resting against the pectoral girdle. As the post-larvae grow the deformity expands ventrally and ultimately also affects the branchiostegal rays, with a bending of the operculum into the gill cavity as a result. Only four aberrant opercular abnormalities were detected after

metamorphosis: a single specimen showed unilateral inwardly folded branchiostegal rays while the operculum did not show the expected associated deformity (Fig. 3C). The operculum, however, showed an abnormal dorsoventral ridge, which probably is a consequence of a previous inward folding. In three post-metamorphic specimens only the dorsocaudal tips of the opercula were severely folded inward and deformed (Fig. 3D).

The mortality rate during the studied rearing period was negligible (0.03%). The prevalence of opercular deformities seems to decrease during metamorphosis (11.0–22.0 TL (Total length), as mentioned by Koumoundouros et al., 1997a) and to increase again afterwards (Fig. 4). The presence of urinary calculi in the gall bladder, which is a typical symptom of stress, showed the same pattern (although not directly correlated, with opercular deformities, $R^2 = 0.067$) (Fig. 4). Of the 383 specimens screened 28.5% showed an opercular deformity, of which 18.3% bilateral. In both datasets there were more left than right deoperculations (osteological

Table 2
Statistics of the discriminant function analyses of the five age classes

Analysis group	Left					Right				
	50 DPH	55 DPH	60 DPH	65 DPH	69 DPH	50 DPH	55 DPH	60 DPH	65 DPH	69 DPH
Wilks' lambda	0.510	0.123	0.428	0.660	0.658	0.577	0.073	0.124	0.711	0.513
χ^2	26.270	39.797	14.437	34.099	30.520	21.418	49.606	35.525	28.009	48.777
df	28	28	28	28	28	28	28	28	28	28
p-level	0.558	0.069	0.984	0.198	0.339	0.808	**0.007**	0.155	0.464	**0.009**
Mahalanobis D^2	4.846	31.610	8.005	3.439	2.570	3.690	55.972	42.377	2.716	4.706
F-value	0.875	1.505	0.178	1.235	1.100	0.666	2.665	0.945	0.975	2.015
df	28, 26	28, 6	28, 4	28, 69	28, 60	28, 26	28, 6	28, 4	28, 69	28, 60
p-level	0.637	0.321	0.998	0.237	0.369	0.853	0.111	0.605	0.514	**0.012**

dataset: $n=21$, of which 33.3% left and 23.8% right deoperculated, external morphology dataset: $n=383$, of which 20.2% left and 13.6% right deoperculated); but only in the external morphology dataset this difference was significant (Fisher's exact test two-tailed p-value$=0.046$). Only in the largest age class (65 DPH) a small significant difference in average length could be observed between normal and deoperculated specimens. ($L_{S \text{ normal}}=17.2\pm$ 1.8 mm, $L_{S \text{ deopere.}}=16.4\pm1.1$ mm, $F_{(79,17)}=2.944$, $p=0.0074$, $T_{(43)}=2.58$, $p=0.013$). Contradictory to these results, the deoperculated specimens in the osteology dataset (juveniles of 110 DPH) were bigger (normal 24.7 ± 1.1 mm L_S; deoperculated 25.3 ± 0.9 mm L_S), but this difference was not significant ($T_{(19)}=$ -0.78738, $p=0.220386$).

3.2. Skeletal shape and deoperculation

The analysis of the osteological dataset yielded two uniform and 36 non-uniform partial warps that were included in the analyses. The consensus configuration, with aligned specimens superimposed (thus showing
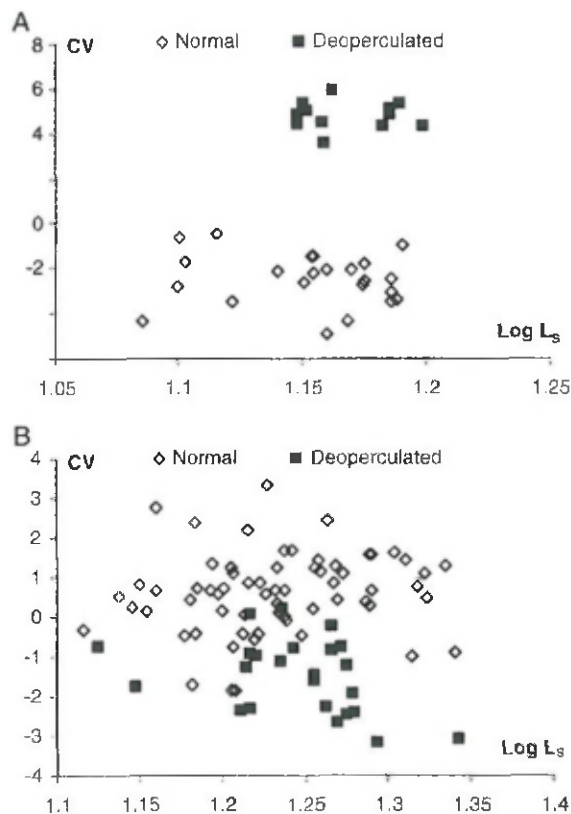

Fig. 9. Scatterplots of the significant canonical variates versus the logarithm of the Standard length (right body side): A. 55 DPH; B. 69 DPH.
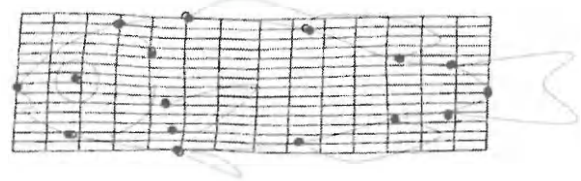

Fig. 10. Deformation grid visualised through TPSRegr, representing the shape difference between a low ($-3,17$) and high ($3,35$) CV-score of the 69 DPH sample. The regression of the shape variables on the CV-scores was subjected to a permutation test (percent unexplained 97.90%, 0.10% Lambda values <-0.00000003, 9.90% Goodall F-values >-1.864).

variation in landmark positions) showed a differential variation in landmark position, with the largest variation in the two landmarks at the posterior border of the opercular bone (Fig. 5). An average of 6.78% of the total variation in the dataset could be attributed to both digitisation and orientation error. The largest digitisation and orientation error were situated at landmark 12 (11.82% of total digitisation error) and landmark 18 (12.33% of total orientation error) respectively. The percentages of variation explained by the relative warps (38 in total) are given in Table 1. The first relative warp, which explained 68.23% of the total shape variation in the dataset, clearly separated the deoperculated and normal configurations, while the other relative warps did not (Fig. 6). Relative warp 1 thus largely represents the shape changes in the head region associated with deoperculation. Besides the expected forward shift of the caudal margin of the opercular and subopercular bone (as observed externally), other more subtle shape differences can be observed. These include an upward shift of the interopercle, angular, quadrate, the infraorbitals and the preopercular. The preorbital region, thus the snout, also shortens with respect to the other landmarks. Most striking of this analysis, however, is the observation that in unilaterally deoperculated specimens, the normal sides show a shape that corresponds perfectly with bilaterally normal specimens, whereas the deoperculated sides showed all the typical shifts in the landmark configuration as in bilaterally deoperculated specimens. Apparently, the prevalence of the deformation associated with deoperculation is completely decoupled bilaterally, thus allowing an astonishing right–left asymmetry.

3.3. Body shape and deoperculation

The shape decomposition of the external morphology data set generated two uniform and 26 non-uniform partial warps. The consensus configuration, with aligned specimens, showed that shape difference is spread all over the body but is situated mainly in the anterior part (head and abdomen). In this analysis, an average of

Table 3
Statistics of the discriminant function analyses of the subsets derived from the total left and right external morphology datasets based on the inflection points

Analysis	Left		Right	
Group	<18.01 mm L_S	>18.01 mm L_S	<17.34 mm L_S	>17.34 mm L_S
Wilks' lambda	0.510	0.123	0.428	0.073
χ^2	26.270	39.797	14.437	49.606
df	28	28	28	28
p-level	0.558	0.069	0.984	0.007
Mahalanobis D^2	4.846	31.610	8.005	55.972
F-value	0.875	1.505	0.178	2.665
df	28, 215	28, 38	28, 199	28, 54
p-level	0.637	0.321	0.998	0.111

28.18% and 17.62% of shape variation could be attributed to digitisation error for the smallest and largest specimen respectively, whereas an average of 9.06% and 16.52% of shape variation could be attributed to orientation errors. The largest digitisation errors are situated at landmark 6 (18.34% of digitisation error) in the smallest and at landmark 9 (9.74%) in the largest specimen. The largest orientation errors were situated in landmark 2 (21.57% of total orientation error) and landmark 1 (19.75%) of the smallest and largest specimen respectively.

None of the relative warps (28 in total) explained shape variation that allowed to distinguish two or more groups. Relative warp 1 (Fig. 7) accounted for 54.00% of the total shape variation in the right side dataset (51.52% in the analysis of the left body sides) and reflects an overall heightening of the body, most extensive in the posterior head region and abdomen, as well as a lengthening of those regions. Because of the higher percentage of variation explained by RW1 for the right side data, the latter will be discussed further where the results of left and right body side analyses are identical. The largest dorsoventral expansion seems to be situated in the posterior margin of the skull and the cleithral region, expanding the nape (the dorsal region between the end of the skull and the beginning of the dorsal fin) and shifting the pectoral and pelvic fins downwards. Because of the expansion of skull and abdomen, the tail region diminishes relatively in size. Relative warp 2 (Fig. 7) explains 9.42% (10.42% in the left analysis) of total shape variation and is characterized by an overall dorsoventral curving of the body, probably as an artefact due to the formalin-fixation.

3.4. Growth allometries and deoperculation

The regression analysis and t-testing for inflection points shows that scores of RW1 of the external

morphology analysis fit nicely onto body size (log-values of L_S) with an allometric shift at 17.34 mm L_S (18.01 mm L_S in the left dataset) (Fig. 8). No apparent differences in the relation between shape and size in normal versus deoperculated specimens could be observed (the inflection points, the intercepts and slopes of the regression lines are very similar, but the R^2-values for the normal specimens, however, were lower).

Five specimens, caught locally at the coast near the hatchery, were included in the analysis for comparison and showed a totally different relationship between shape (RW1) and size (Log L_S) (Fig. 8): the wild caught specimens obtained the same RW1-scores (thus had a comparable shape) as reared specimens of a much smaller size (17.3–18.1 mm L_S versus 13.3 mm L_S), possibly indicating an accelerated growth-development relationship under intensive rearing conditions.

It is only in the 69 DPH age class that a significant difference between the normal and deoperculated cluster was observed, after a discriminant function analysis based on the shape variables of the right side (χ^2-test, $p<0.01$) (Table 2, Fig. 9B). Still, a clear separation or at least a strong polarization of the canonical variate scores of the two clusters was observed in all age classes. As example, in the 55 DPH sample (Fig. 9A), the difference was clear in a plot of the scores but not significant ($F_{(28,6)}=4.147$, $p=0.0872$, $D^2=139.97$).

The shifts in body shape associated with deoperculation at 69 DPH are minor with the largest differences involving a reduced abdominal height (more specifically at the nape) and a posterior shortening of the lower jaw (Fig. 10).

Finally, we separated the total datasets ($n=310$) of left and right external morphology in two subsets each, based on their inflection points, but the discriminant function analyses of these subsets didn't reveal significant discriminations between normal and deoperculated specimens (Table 3).

4. Discussion

Both datasets showed the occurrence of more left than right deoperculations (osteological dataset: $n=21$, of which 33.3% left and 23.8% right deoperculated; external morphology dataset: $n=383$, of which 20.2% left and 13.6% right deoperculated). Only for the external morphology dataset this difference was significant (Fisher's exact test two-tailed p-value = 0.046). Earlier studies on opercular deformities in sea bream all concluded that unilateral deformation was side-independent and thus was the result of a fluctuating asymmetry model (Koumoundouros et al., 1997a; Galeotti et al., 2000; Beraldo et al., 2003). Our data on the other hand suggest a directional asymmetry model. Fluctuating asymmetry is believed to be a consequence of environmental factors that have an effect on developmental instability during the early life stages (Adams and Niswander 1967; Barahona-Fernandes, 1982), while directional asymmetry is believed to be an inherited factor. Existing literature on the genetic influence are contradictory: according to Tave and Handwerker (1994) opercular deformities are non-inheritable in *Oreochromis niloticus*, while inbreeding in *Cichlasoma nigrofasciatum* resulted in more opercular deformities (Winemiller and Taylor, 1982). A basic assumption of asymmetry research is that left and right side experience identical environmental factors. This may not be the case under rearing conditions: intensive schooling in circular tanks for example may cause a different development of the sides of the body.

The prevalence of higher left deoperculation numbers in the samples studied, remains to be confirmed by additional analysis focusing on the pattern behind the asymmetry.

The transformations co-occurring with opercular deformities are not only affecting the operculum itself, but also the surrounding cranial structures. Major shape changes related with deoperculation seem to be concentrated in the posteroventral region of the skull, with an anterodorsally directed shift. Additionally, such a shift is observed in the postorbital region and the mandibular arch. Whether both transformations share the same causal factor (*e.g.* gene expression pattern), are spatially interrelated, or even have independent causes, remains to be studied.

The most striking observations of the cranial deformations are that in unideoperculated specimens the deoperculated side shows identical transformations, with the same intensity, as both sides in bideoperculated specimens, while the normal side has an identical morphology to that of normal (bioperculated) specimens. Consequently, it can be suggested that both in unilaterally and bilaterally deoperculated larvae, the morphogenetic pattern genera-

ting the normal and/or deformed side on the contralateral faces in the skull is completely independent (at least with respect to deoperculation).

We could not fully confirm the results of Chatain (1994) and Koumoundouros et al. (1997a), that opercular deformities affect larval size (or are at least related to it). A minor but significant size difference could only be observed in the 65 DPH sample, where normal specimens were slightly larger.

The most important ontogenetic allometries (represented by relative warp one) of the normal and deoperculated groups shared a comparable slope and intercept, as well as they both experienced a clear inflection point at $17.1–18.0$ mm L_S, which is situated at the end of the metamorphosis period ($11.0–22.0$ TL) as mentioned by Koumoundouros et al. (1997a). Geometric morphometrics can be an important asset in defining the exact demarcations of metamorphic phases (as in several invertebrates) in organisms with a less pronounced metamorphosis such as gilthead sea bream. Frequently, single morphological characters are used to demarcate the onset of a specific early life history phase, such as the formation of fin rays or the completion of the fin ray formation (see for example Balon, 1975). Other studies do involve changes in allometric variables (*e.g.* Koumoundouros et al., 1995). Whether or not *S. aurata* undergoes a true phase of metamorphosis can be argued about. In any case, this study indicates the existence of marked shifts in the pattern of their ontogenetic shape changes at about 17 mm L_S.

Koumoundouros et al. (1997a) described a temporary stasis in the presence of opercular deformities during metamorphosis. Our results, on the contrary, even indicate a decrease in the rate of deoperculation during metamorphosis, while mortality was negligible during the studied stages (0.03%). Deoperculated specimens can regenerate their damaged opercula to a great extent during later development, as described by De Wolf et al. (2004). Therefore it is likely that regeneration may also occur during metamorphosis. The four aberrant opercular abnormalities, which were only encountered after metamorphosis, could be the result of an incomplete recovery. This remains to be verified, however.

Chatain (1994) microscopically observed the earliest opercular deformities at $12–15$ mm TL. We could detect opercular deformations microscopically from 8.0 mm L_S and 40 DPH on, as a local shortening (or possible inward folding) of the dorsal opercular edge. However, earlier microscopical discrimination is very likely to be possible, as these specimens were the youngest and smallest stages examined. The use of bone-staining and histological methods allowed the identification of

Faustino, M., Power, D.M., 2000. Osteologic development of the viscerocranial skeleton in sea bream: alternative ossification strategies in teleost fish. J. Fish Biol. 58, 537–572.

Francescon, A., Freddi, A., Barbaro, A., Giavenni, R., 1988. Daurade *Sparus aurata* L. reproduite artificiellement et daurade sauvage. Expériences paralleles en diverses conditions d'élevage. Aquaculture 72, 273–285.

Furuita, H., Tanaka, H., Yamamoto, T., Shiraishi, M., Takeuchi, T., 2000. Effects of n-3 HUFA levels in broodstock diet on the reproductive performance and egg and larval quality of the Japanese flounder, *Paralichthys olivaceus*. Aquaculture 187, 387–398.

Fishery Information, Data and Statistics Unit, Food and Agriculture Organization of the United Nations (FAO), 2005. FISHSTAT Plus: Universal software for fishery statistical time series, version 2.3. (available on-line at http://www.fao.org/fi/statist/FISOFT/FISHPLUS.asp).

Galeotti, M., Beraldo, P., de Dominis, S., D'Angelo, L., Ballestrazzi, R., Musetti, R., Pizzolito, S., Pinosa, M., 2000. A preliminary histological and ultrastructural study of opercular anomalies in gilthead sea bream (*Sparus aurata*). Fish Phys. Biochem. 22, 151–157.

Hanken, J., Wassersug, R., 1981. The visible skeleton. A new double-stain technique reveals the native of the 'hard' tissues. Funct. Photogr. 16, 22–26.

Koumoundouros, G., Kiriakos, Z., Divanach, P., Kentouri, M., 1995. Morphometric relationships as criteria for the evaluation of larval quality of gilthead sea bream. Aquacult. Int. 3, 143–149.

Koumoundouros, G., Oran, G., Divanach, P., Stefanakis, S., Kentouri, M., 1997a. The opercular complex deformity in intensive gilthead sea bream (*Sparus aurata* L.) larviculture. Moment of apparition and description. Aquaculture 156, 165–177.

Koumoundouros, G., Gagliardi, F., Divanach, P., Boglione, C., Cataudella, S., Kentouri, M., 1997b. Normal and abnormal osteological development of caudal fin in *Sparus aurata* L. fry. Aquaculture 149, 215–226.

Koumoundouros, G., Kouttouki, S., Georgakopoulou, E., Papadakis, I., Maingot, E., Kaspiris, P., Kiriakou, Y., Georgiou, G., Divanach, P., Kentouri, M., Mylonas, C.C., 2005. Ontogeny of the shi drum *Umbrina cirrosa* (Linnaeus 1758), a candidate new species for aquaculture. Aquacult. Res. 36, 1265–1272.

Lindesjöö, E., Thulin, J., Bengtsson, B.E., Tjaernlund, U., 1994. Abnormalities of a gill cover bone, the operculum, in perch *Perca fluvialitis* from a pulp mill effluent area. Aquat. Toxicol. 28, 189–207.

Loy, A., Mariani, L., Bertelletti, M., Tunesi, L., 1998. Visualizing allometry: geometric morphometrics in the study of shape changes in the early stages of the two-banded sea bream, *Diplodus vulgaris* (Perciformes, Sparidae). J. Morphol. 237, 137–146.

Loy, A., Boglione, C., Cataudella, S., 1999. Geometric morphometrics and morpho-anatomy: a combined tool in the study of sea bream (*Sparus aurata*, Sparidae) shape. J. Appl. Ichthyol. 15, 104–110.

Loy, A., Boglione, C., Gagliardi, F., Ferrucci, L., Cataudella, S., 2000. Geometric morphometrics and internal anatomy in sea bass shape analysis (*Dicentrarchus labrax* L., Moronidae). Aquaculture 186, 33–44.

Loy, A., Bertelletti, M., Costa, C., Ferlin, L., Cataudella, S., 2001. Shape changes and growth trajectories in the early stages of three species of the genus *Diplodus* (Perciformes, Sparidae). J. Morphol. 250, 24–33.

Mourente, G., Rodriguez, A., Tocher, D.R., Sargent, J.R., 1993. Effects of dietary docosahexaenoic acid (DHA 22/6N-3) on lipid and fatty-acid compositions and growth in gilthead sea bream (*Sparus aurata* L.) larvae during first feeding. Aquaculture 112, 79–98.

Papandroulakis, N., Divanach, P., Kentouri, M., 2002. Enhanced biological performance of intensive sea bream (*Sparus aurata*) larviculture in the presence of phytoplankton with long photophase. Aquaculture 204, 45–63.

Paperna, I., 1978. Swimbladder and skeletal deformations in hatchery bred *Sparus aurata*. J. Fish Biol. 12, 109–114.

Parra, G., Yufera, M., 2000. Feeding, physiology and growth responses in first-feeding gilthead sea bream (*Sparus aurata* L.) larvae in relation to prey density. J. Exp. Mar. Biol. Ecol. 243, 1–15.

Polo, A., Yufera, M., Pascual, E., 1991. Effects of temperature on egg and larval development of *Sparus aurata* L. Aquaculture 92, 367–375.

Richtsmeier, J.T., DeLeon, V.B., Lele, S.R., 2002. The promise of geometric morphometrics. Yearb. Phys. Anthropol. 45, 63–91.

Rohlf, F.J., 1993. Relative warp analysis and an example of its application to mosquito wings. In: Marcus, L.F., Bello, E., García-Valdecasas, A. (Eds.), Contributions to Morphometrics. C.S.I.C., Madrid, pp. 131–159.

Rohlf, F.J., 1996. Morphometric space, shape components and the effects of linear transformations. In: Marcus, L.F., Corti, M., Loy, A., Naylor, G.J.P., Slice, D.E. (Eds.), Advances in Morphometrics. Plenum Press, New York, pp. 117–129.

Rohlf, F.J., 2003. TpsSmall: Thin Plate Spline Small Variation (Version 1.20). State University of New York at Stony Brook, Stony Brook, New York.

Rohlf, F.J., 2004a. TpsUtil: Thin Plate Spline Utility (Version 1.33). State University of New York at Stony Brook, Stony Brook, New York.

Rohlf, F.J., 2004b. TpsDig: Thin Plate Spline Digitise (Version 1.40). State University of New York at Stony Brook, Stony Brook, New York.

Rohlf, F.J., 2004c. TpsRegr: Thin Plate Spline Shape Regression (Version 1.29). State University of New York at Stony Brook, Stony Brook, New York.

Rohlf, F.J., 2005. TpsRelw: Thin Plate Spline Relative Warp Analysis (Version 1.41). State University of New York at Stony Brook, Stony Brook, New York.

Rohlf, F.J., Slice, D.E., 1990. Extensions of the Procrustes method for the optimal superimposition of landmarks. Syst. Zool. 39, 40–59.

Rohlf, F.J., Marcus, L.F., 1993. A revolution in morphometrics. Trends Ecol. Evol. 8, 129–132.

Rohlf, F.J., Loy, A., Corti, M., 1996. Morphometric analysis of old world Talpidae (Mammalia, Insectivora) using partial-warp scores. Syst. Biol. 45, 344–362.

Sadek, S., Osman, M.F., Mansour, M.A., 2004. Growth, survival and feed conversion rates of sea bream (*Sparus aurata*) cultured in earthen brackish water ponds fed different feed types. Aquacult. Int. 12, 409–421.

Tandler, A., Helps, S., 1985. The effects of photoperiod and water exchange-rate on growth and survival of gilthead sea bream (*Sparus aurata*, Linnaeus, Sparidae) from hatching to metamorphosis in mass rearing systems. Aquaculture 48, 71–82.

Tave, D., Handwerker, T.S., 1994. Semi-operculum: A non-heritable birth defect in *Tilapia nilotica*. J. World Aquac. Soc. 25, 333–336.

Taylor, W.R., Van Dyke, G.C., 1985. Revised procedures for staining and clearing small fishes and other vertebrates for bone and cartilage study. Cybium 9, 107–119.

Valentin, A., Sévigny, J.M., Chanut, J.P., 2002. Geometric morphometrics reveals body shape differences between sympatric redfish *Sebastes mentalla*, *Sebastes fasciatus* and their hybrids in the Gulf of St Lawrence. J. Fish Biol. 60, 857–875.

Van Snik, G.M.K., Van den Boogaart, J.G.M., Osse, J.W.M., 1997. Larval growth patterns in *Cyprinus carpio* and *Clarias gariepinus* with attention to the finfold. J. Fish Biol. 50, 1339–1352.

Winemiller, K.O., Taylor, D.H., 1982. Inbreeding depression in the convict cichlid, *Cichlasoma nigrofasciatum* (Baird and Girard). J. Fish Biol. 21, 399–402.

opercular deformities at 6.1 mm TL (Koumoundouros et al., 1997a) and 17 DPH (Galeotti et al., 2000) in earlier studies, but these methods are unpractical in daily quality assessment in commercial hatcheries. Koumoundouros et al. (1997a) proposed a metrical method to quantify and distinguish opercular deformities during and after metamorphosis for quality assessment and experimentation on the causative factors. This method is based on the ratio of (1) the length from the posterior margin of the eye to the posterior margin of the operculum (pstOr) and the sum of (2) the eye diameter (ED) and (3) the length from the tip of the snout to the anterior margin of the eye (prOr) (thus ratio = pstOr/(prOr + ED)). Koumoundouros et al. (1995) also proposed several classic morphometric ratios (for example head length on TL) for the daily assessment of larval quality.

Our method, a discriminant function analysis performed on the shape variables obtained through landmark-based geometric morphometrics, could significantly separate deoperculated from normal specimens at 69 DPH, based on small shape differences of the external morphology. Our preliminary analysis, however, suggests that deoperculated specimens can be detected much earlier using geometric morphometrics (more specimens need to be analyzed, however, to support this statistically). An automated geometric morphometric method of the external morphology (e.g. based on Fourier analysis) could thus be a reliable, time and cost efficient method for quality assessment of reared fish stocks.

5. Conclusion

This preliminary study, using geometric morphometrics to detect and analyse opercular deformations in *S. aurata*, has yielded some new insights in the problem. First, the methodology proves to be very useful for understanding the nature of cranial deformations that occur in association with opercular deformations, as well as for screening for shape changes related to it (both in the external and the skeletal morphology). Second, it has been shown that there exists a striking left–right independency towards deoperculation. Third, even though a subtle size difference was observed at 65 DPH in normal and deoperculated specimens, allometries during growth appear to be very similar in normal and deoperculated specimens.

Further sampling, however, is needed to test some of the observations, as well as to expand the size range in order to evaluate the earliest possible detection of opercular deformities in *S. aurata*, from which an easy detection protocol could be derived. Further testing of these observations with experimental setups will also be needed in order to understand causal factors behind deoperculation.

References

Adams, M.S., Niswander, J.D., 1967. Developmental 'noise' and congenital malformation. Gen. Res. Comp. 10, 313–317.

Adams, D.C., Rohlf, F.J., Slice, D.E., 2004. Geometric morphometrics: ten years of progress following the 'revolution'. Ital. J. Zool. 71, 5–16.

Alfonso, J.M., Montero, D., Robaina, L., Astorga, N., Izquierdo, M.S., Gines, R., 2000. Association of lordosis–scoliosis–kyphosis deformity in gilthead sea bream (*Sparus aurata*) with family structure. Fish Physiol. Biochem. 22, 159–163.

Andrades, J.A., Becerra, J., Fernández-Llebrez, P., 1996. Skeletal deformities in larval, juvenile and adult stages of cultured gilthead sea bream (*Sparus aurata* L.). Aquaculture 141, 1–11.

Arnqvist, G., Mårtensson, T., 1998. Measurement error in geometric morphometrics: empirical strategies to assess and reduce its impact on measures of shape. Acta Zool. Hung. 44, 73–96.

Balon, E.K., 1975. Terminology of intervals in fish development. J. Fish. Res. Board Can. 32, 1663–1670.

Barahona-Fernandes, M.H., 1982. Body deformation in hatchery reared European sea bass *Dicentrarchus labrax* (L.). Types, prevalence and effect on fish survival. J. Fish Biol. 21, 239–249.

Beraldo, P., Pinosa, M., Tibaldi, E., Canavese, B., 2003. Abnormalities of the operculum in gilthead sea bream (*Sparus aurata*): morphological description. Aquaculture 220, 89–99.

Boglione, C., Cagliardi, F., Scardi, M., Cataudella, S., 2001. Skeletal descriptors and quality assessment in larvae and post-larvae of wild-caught and hatchery-reared gilthead sea bream (*Sparus aurata* L. 1758). Aquaculture 192, 1–22.

Bookstein, F.L., 1990. Introduction to methods for landmark data. In: Rohlf, F.J., Bookstein, F.L. (Eds.), Proceedings of the Michigan Morphometrics Workshop, pp. 215–225.

Cahu, C., Infante, J.Z., Takeuchi, T., 2003. Nutritional components affecting skeletal development in fish larvae. Aquaculture 227, 245–258.

Cavalcanti, M.J., Monteiro, L.R., Lopes, P.R.D., 1999. Landmark-based morphometric analysis in selected species of serranid fishes (Perciformes: Teleostei). Zool. Stud. 38, 287–294.

Chatain, B., 1994. Estimation et amélioration des performances zootechniques de l'élevage larvaire de *Dicentrarchus labrax* et de *Sparus aurata*. Thèse Doctorale en Sciences, Université d'Aix-Marseille II, 199 pp.

Chatain, B., Ounais-Guschemann, N., 1990. Improved rate of initial swimbladder inflation in intensively reared *Sparus aurata*. Aquaculture 84, 345–353.

De Wolf, T., Courtens, V., Capiferri, U., Pirone, A., Lenzi, C., Lenzi, F., 2004. The influence of light conditions on the operculum recovery of sea bream (*Sparus aurata* L.) fry. Book of abstracts. Aquaculture Europe 2004, Biotechnologies for quality, Barcelona, Spain 20–23 October, 2004, p. 292.

Dodson, P., 1978. On the use of ratios in growth studies. Syst. Zool. 27, 62–67.